Atmos. Chem. Phys., 17, 4115–4130, 2017
www.atmos-chem-phys.net/17/4115/2017/
doi:10.5194/acp-17-4115-2017

Atmospheric Chemistry and Physics Open Access EGU

Day and night-time formation of organic nitrates at a forested mountain site in south-west Germany

Nicolas Sobanski, Jim Thieser, Jan Schuladen, Carina Sauvage, Wei Song, Jonathan Williams, Jos Lelieveld, and John N. Crowley

Max-Planck-Institut für Chemie, Division of Atmospheric Chemistry, Mainz, Germany

Correspondence to: John N. Crowley (john.crowley@mpic.de)

Received: 30 September 2016 – Discussion started: 8 November 2016
Revised: 7 February 2017 – Accepted: 6 March 2017 – Published: 27 March 2017

Abstract. We report in situ measurements of total peroxy nitrates (ΣPNs) and total alkyl nitrates (ΣANs) in a forested–urban location at the top of the Kleiner Feldberg mountain in south-west Germany. The data, obtained using thermal dissociation cavity ring-down spectroscopy (TD-CRDS) in August–September 2011 (PARADE campaign) and July 2015 (NOTOMO campaign), represent the first detailed study of ΣPNs and ΣANs over continental Europe. We find that a significant fraction of NO_x (up to 75 %) is sequestered as organics nitrates at this site. Furthermore, we also show that the night-time production of alkyl nitrates by reaction of NO_3 with biogenic hydrocarbons is comparable to that from daytime OH-initiated oxidation pathways. The ΣANs / ozone ratio obtained during PARADE was used to derive an approximate average yield of organic nitrates at noon from the OH initiated oxidation of volatile organic compounds (VOCs) of ∼ 7 % at this site in 2011, which is comparable with that obtained from an analysis of VOCs measured during the campaign. A much lower AN yield, < 2 %, was observed in 2015, which may result from sampling air with different average air mass ages and thus different degrees of breakdown of assumptions used to derive the branching ratio, but it may also reflect a seasonal change in the VOC mixture at the site.

1 Introduction

The gas- and aerosol-phase chemistry of the continental, tropospheric boundary layer is strongly influenced by reactive nitrogen oxides. The primary pollutants NO and NO_2 (constituting the NO_x family) are mostly emitted by anthropogenic activity involving high-temperature combustion or from microbial activity in soils, and they have a strong impact on tropospheric O_3 levels. Knowing the fate of NO_x is paramount to prediction of O_3 production rates and oxidation capacity on regional and global scales (Lelieveld et al., 2016). Following emission, NO undergoes a series of reaction steps that ultimately lead either to the formation of short-lived trace gases that can act as sinks for NO_x (e.g. HNO_3) or to the formation of longer-lived reservoir species that can be transported over long distances and act as a source of NO_x (e.g. $RONO_2$ and $RC(O)OONO_2$) in locations that are remote from anthropogenic emissions. In the troposphere, a significant amount of NO_x can be temporarily sequestered as organic nitrates. HNO_3 is produced predominantly by the oxidation of NO_2 by OH, whereas organic nitrates are produced by the oxidation of both NO and NO_2 by organic peroxy radicals during the day (Reactions R3 and R4) or in the oxidation of alkenes by NO_3 during the night (Reaction R6) to produce peroxy radicals that subsequently produce stable organonitrates by any radical terminal Reaction (R7). Organic peroxy radicals are formed in the oxidation of hydrocarbons by OH (Reactions R1 and R2) (Atkinson, 2000; Atkinson and Arey, 2003a, b).

The products of NO_x oxidation by organic radicals are peroxy nitrates (RO_2NO_2, abbreviated as PNs; Reaction R3) and alkyl nitrates ($RONO_2$, abbreviated as ANs; Reaction R4). Based on thermal lifetimes, PNs may be divided in two families, those with a carbonyl group adjacent to the peroxy entity (i.e. $RC(O)O_2NO_2$) and those without. The former are peroxyacyl nitric anhydrides, generally referred to as peroxyacyl nitrates or PANs, and have lifetimes with respect to thermal dissociation on the order of hours in the midlatitude bound-

ary layer. Non-acyl PNs (RO_2NO_2) such as $CH_3O_2NO_2$ and HO_2NO_2 thermally decompose on timescales of seconds to minutes at temperatures close to 298 K and are thus only encountered in significant concentrations in cold regions of the atmosphere (Murphy et al., 2004; Browne et al., 2011; Nault et al., 2015). Alkyl nitrates are formed with variable branching ratio in a minor channel (Reaction R4) of the reaction between organic peroxy radicals and NO, the greater fraction of this reaction leading to the formation of an alkoxy radical and NO_2 (Reaction R5) and thus (via NO_2 photolysis) ultimately to O_3 formation. Alkyl nitrates are also formed at night during the NO_3-induced oxidation of unsaturated hydrocarbons. The first reaction step is the addition of NO_3 to a double bond followed by formation of a nitrooxy alkylperoxy radical (Reaction R6), the fate of which includes reaction with HO_2, other peroxy radicals, NO_3, NO_2, or if available, NO, so that the final products are, hydroxy-, hydroxide-, and carbonyl-substituted nitrates and dinitrates (Schwantes et al., 2015; IUPAC, 2016). The nitrate yields (per VOC reacted) can be high, especially for biogenic VOCs including the terpenoids, and can exceed 50 % (Ng et al., 2017).

Organic nitrates have highly variable lifetimes (from seconds to days) that are mainly controlled by rates of thermal decomposition and thus temperature for PNs. For ANs, OH oxidation, photolysis, deposition, or scavenging by aerosol particles, all play a role (Roberts, 1990; Browne et al., 2013; Rollins et al., 2013).

$$\mathrm{OH + RH(+O_2) \rightarrow RO_2 + H_2O} \quad \text{(R1)}$$

$$\mathrm{R = R' + OH(+O_2) \rightarrow R(OH)R'O_2} \quad \text{(R2)}$$

$$\mathrm{RO_2 + NO_2 + \mathit{M} \rightarrow RO_2NO_2 + \mathit{M}} \quad \text{(R3)}$$

$$\mathrm{RO_2 + NO + \mathit{M} \rightarrow RONO_2 + \mathit{M}} \quad \text{(R4)}$$

$$\mathrm{RO_2 + NO \rightarrow RO + NO_2} \quad \text{(R5)}$$

$$\mathrm{R = R' + NO_3(+O_2) \rightarrow R(ONO_2)R'O_2} \quad \text{(R6)}$$

$$\mathrm{R(ONO_2)R'O_2(+RO_\mathit{x}, NO_\mathit{x}) \rightarrow ANs} \quad \text{(R7)}$$

The first field measurements of organic nitrates were made using low-time-resolution methods (gas chromatography) (Roberts et al., 1989; Blanchard et al., 1993) and focused mostly on PAN (peroxy acetyl nitrate, $CH_3C(O)O_2NO_2$), PPN (peroxy propyl nitrate, $C_2H_5C(O)O_2NO_2$), and MPAN (methacryloyl peroxynitrate, $CH_3C(CH_2)C(O)O_2NO_2$) (Williams et al., 1997, 2000), which are the most common peroxy nitrates in the continental boundary layer, and individual mono- and polyfunctional alkyl nitrates from alkane or alkene precursors (Atlas, 1988; Flocke et al., 1991). More recently, mass-spectrometry-based methods have been developed to measure a wider range of organic nitrates at high time resolution (Beaver et al., 2012; B. H. Lee et al., 2016). Early attempts to compare total reactive nitrogen NO_y (where $NO_y = NO_x + RO_2NO_2 + RONO_2 + HNO_3 + HONO$ ++) with the sum of individually measured species (Fahey et al., 1986; Buhr et al., 1990; Ridley et al., 1990) revealed that a substantial fraction of NO_y was missing. This phenomenon was addressed by the first measurements of total peroxynitrates (ΣPNs) and total alkyl nitrates (ΣANs) by thermal dissociation coupled with laser-induced fluorescence detection of NO_2 (Day et al., 2003). Those and subsequent measurements (Wooldridge et al., 2010; Perring et al., 2013) indicated that, depending on environment, the interaction between NO_x and VOCs leads to a wide variety of compounds with different levels of structural functionality and atmospheric lifetime and they can have a variable and significant influence on the lifetime of NO_x and particle composition (Browne et al., 2013; Ayres et al., 2015).

We present here an analysis of organic nitrates and NO_2 measured using thermal dissociation cavity ring-down spectroscopy (TD-CRDS) during two field campaigns that took place at a forested, semi-rural mountain site in south-western Germany. As far as we are aware, this work constitutes the first measurement and analysis of ΣPNs and ΣANs over continental Europe. We show that the daily variations of ΣANs and ΣPNs are controlled by photochemical oxidation of VOCs, night-time production by NO_3-induced oxidation of biogenic VOCs, and local meteorology. We report an estimation of the effective branching ratios and α(OH) of OH-induced AN formation using O_3 measurements, and we compare this with an estimation based on VOCs at the site and known individual branching ratios. The results from the two campaigns are compared and differences are discussed in terms of annual and seasonal changes in meteorology and VOC (biogenic and anthropogenic).

2 Campaign site and meteorology

The August–September 2011 PARADE campaign (PArticles and RAdicals: Diel observations of the impact of urban and biogenic Emissions) and the July 2015 NOTOMO campaign (NOcturnal chemistry at the Taunus Observatory: insights into Mechanisms of Oxidation) both took place at the Taunus Observatory (50.22° N, 8.45° E) on top of the Kleiner Feldberg mountain, 850 m above sea-level and 500 m above nearby urban centres in the states of Hesse and Rhineland-Palatinate in south-western Germany. This site has been described extensively in different publications (Crowley et al., 2010; Sobanski et al., 2016b) and only a short description is given here. A few kilometres to the N-NE and SE of the station are two mountains of similar height (Großer Feldberg 878 m and Altkönig 798 m a.s.l.). The nearby (tens of kilometres) environment in the complete northern sector is a partially forested, rural region. The SW-SE sector is a more densely populated, industrialized region that includes the Frankfurt–Mainz–Wiesbaden urban agglomeration. Frankfurt is situated $\approx$ 20 km to the SE and Mainz and Wiesbaden $\approx$ 20–30 km to the SW. A detailed land-use analysis of the surrounding area was given by Sobanski et al. (2016b).

Reactive trace-gas measurements at the site are strongly influenced by the horizontal advection of different types of

air masses, both on a local scale (forest–rural vs. urban) and on regional scales (continental vs. marine). On some nights during PARADE, the instruments sampled air from a low-lying residual layer, which resulted in very high NO_3 steady-state lifetimes ($\approx$ 1 h). Otherwise, the NO_3 lifetimes were generally less than 10 min (Sobanski et al., 2016b).

During both campaigns, the meteorological conditions were very variable and were associated with different air mass origins. The PARADE campaign can be divided into three periods (Phillips et al., 2012). The first period from 15 to 26 August was influenced by air masses of continental origin and was associated with high temperature and low humidity. A cold front arriving from the west resulted in 2 consecutive days of rain–fog conditions and a large decrease in temperature and ozone. The period from 26 to 5 September was influenced by advection from the Atlantic–UK region and during this period the temperature increased progressively together with ozone. A second cold front on 5 September again resulted in a fast temperature decrease followed by a period of low photochemical activity. The NOTOMO campaign was characterized by frequent fluctuation between cold–wet and warm–dry periods. Back trajectory calculations (48 h) showed that the warm–dry periods were generally associated with air masses of continental origin, and the cold–wet periods with air masses from the west with Atlantic influence.

3 Instrumentation

The instruments deployed during both field campaigns have been described in Schuster et al. (2009) and Thieser et al. (2016) for PARADE and in Sobanski et al. (2016a) for NOTOMO. During the PARADE campaign, all instruments used collocated inlets of perfluoralkoxy (PFA) piping. During the NOTOMO campaign, the instruments described here sampled from a common, high-volume flow inlet. Temperature, wind speed, and wind direction data during NOTOMO were measured by the permanent instrumentation of the Hessian Agency for Nature Conservation, Environment and Geology (HLNUG) at this site.

3.1 NO_2, NO_3, ΣPNs, and ΣANs

NO_2 and total gas-phase organic nitrates were measured by TD-CRDS during both campaigns. Membrane filters were used to prevent aerosol from entering the cavity ring-down (CRD) inlets, which would lead to severe reductions in the detection limit, degradation of the cavity mirrors, and also to the detection of particulate nitrate (both organic and inorganic) in the thermal dissociation (TD) channels.

3.1.1 PARADE

During PARADE, a two-cavity TD-CRDS instrument was deployed (Thieser et al., 2016). The instrument was located in a container and sampled air from 5 m long PFA tube (1/2 in outer diameter) acting as a bypass flow through which ambient air was drawn at $\sim$ 40 SLM (standard litres per minute). The Teflon-coated (DuPont, FEP, TE 9568) cavities were operated at 405 and 409 nm, and both were maintained at 35 °C to improve thermal stability. One cavity sampled air from the bypass flow at ambient temperature to measure NO_2 mixing ratios. The second channel sampled alternately through two heated inlets, one held at 200 °C and the other at 450 °C, to thermally dissociate PNs and ANs respectively into NO_2. When sampling through the 200 °C inlet, this channel measures the sum of ambient $NO_2 + \Sigma$PNs. Sampling via the 450 °C inlet results in detection of $NO_2 + \Sigma$PNs + ΣANs. Mixing ratios of ΣPNs and ΣANs were obtained by the difference in NO_2 measured in the two cavities and by applying corrections to account for conversion (to NO_2) of $ClNO_2$ (measured by chemical ionization mass spectrometry; Phillips et al., 2012) and N_2O_5 (TD-CRDS, Sobanski et al., 2016b) in the hot inlets and also for biases related to reactions involving peroxy radicals, NO, NO_2, and O_3, as outlined in detail in Thieser et al. (2016). The average correction factor for the ANs was 1.2, with maximum values of 2. The uncertainty associated with the correction procedure is estimated as $\sim$ 30 % (Thieser et al., 2016).

During PARADE, NO_3 was measured by the 662 nm two-channel TD-CRDS described in Schuster et al. (2009). One cavity sampled air at ambient temperature and measured NO_3, the second one measured the sum of NO_3 and N_2O_5 following the thermal dissociation of N_2O_5 to NO_3 and NO_2 at 100 °C. This instrument was located on the rooftop and sampled air from the centre of a bypass flow (50 SLM) through a 1 m long, 1/2 in (12.7 mm) diameter PFA pipe. The detection limits for NO_3 and NO_2 were 2 and 30 pptv and the uncertainties were 15 and 6 % respectively. As described in Thieser et al. (2016), the uncertainty associated with the NO_2 measurement is 6 % + 20 pptv $\times$ RH/100 (where RH is the relative humidity in %). The detection limit and uncertainties for the organic nitrate measurements depend on NO_x levels and the reader is referred to Thieser et al. (2016) for more details.

3.1.2 NOTOMO

The five-channel TD-CRDS deployed during the NOTOMO campaign was recently described in detail by Sobanski et al. (2016a). This instrument has five identical cavities sampling from separate inlet lines. Two cavities operate at 662 nm for the detection of NO_3, and the other three operate at 405 nm to detect NO_2. One 662 nm cavity samples 8 SLM from an inlet at ambient temperature to measure NO_3, while the other draws 7 SLM through an inlet at 110 °C to

Table 1. VOCs measured during the PARADE campaign by GC-MS–FID.

VOC	Mean noon mixing ratio (pptv)	k_{OH+VOC} (cm^3 $molecule^{-1}$)	α(OH)	P(ANs) (pptv h^{-1})	$P(O_3)$ (pptv h^{-1})
limonene	28	1.71×10^{-10}	0.23	11.89	74.5
myrcene	20	2.15×10^{-10}	0.23	10.68	76.2
α-pinene	49	5.37×10^{-11}	0.18	5.12	66.4*
isoprene	85	1.01×10^{-10}	0.07	6.49	177.3
Sum BVOCs				34.18	394.3
ethylbenzene	26	7.10×10^{-11}	0.072	1.44	36
n-Pentane	211	3.9×10^{-12}	0.105	0.93	23*
i-pentane	282	3.9×10^{-12}	0.07	0.83	22*
p-xylene	46	1.43×10^{-11}	0.097	0.69	13
n-Butane	265	2.54×10^{-12}	0.077	0.56	19*
hexane	56	5.61×10^{-12}	0.141	0.56	8.3*
m-xylene	46	1.43×10^{-11}	0.074	0.53	13
propene	105	2.63×10^{-11}	0.015	0.45	58
benzene	78	1.23×10^{-11}	0.034	0.35	19
i-Butane	131	2.33×10^{-112}	0.096	0.32	7*
cis-2-Butene	15	5.6×10^{-11}	0.034	0.31	17
o-xylene	21	1.37×10^{-11}	0.081	0.25	5.8
toluene	126	6.0×10^{-12}	0.029	0.24	15
ethene	246	8.5×10^{-12}	0.0086	0.19	45
propane	330	1.15×10^{-12}	0.036	0.15	7.9
methane	1.8×10^6	6.9×10^{-15}	0.0005	0.07	268
ethane	590	2.6×10^{-13}	0.019	0.033	3.3
HCHO	1940	8.5×10^{-12}	0	0	358
CO	1.2×10^5	2.4×10^{-13}	0	0	303
Sum AVOCs				7.9	1071.1
Sum				42.1	1465.4

BVOCs are mainly biogenically emitted VOCs and AVOCs are mainly anthropogenically emitted VOCs. The production rate of alkyl nitrates and O_3 is calculated based on an OH concentration of 3×10^6 molecule cm^{-3}. Values of α(OH) were taken from Perring et al. (2013), and values of k_{OH+VOC} were taken from Atkinson and Arey (2003a). * The number of ozone molecules produced per VOC oxidized is 2.85 (all others are 2) (Rosen et al., 2004).

measure the sum of $NO_3 + N_2O_5$ following thermal dissociation of N_2O_5 to NO_3. Of the three 405 nm cavities, one draws 2.5 SLM via an inlet at ambient temperature to measure NO_2, and the other two each sample 2.5 SLM from inlets heated to 175 and 375 °C to measure $NO_2 + \Sigma$PNs and $NO_2 + \Sigma$PNs $+ \Sigma$ANs respectively. The 1/4 in (6.35 mm) inlet line for the 662 nm cavities was attached with a T-piece to a 60 cm long 1/2 inch PFA pipe sampling air at 100 L min^{-1} from the centre of a large diameter (15 cm), high-flow inlet (10 m^3 min^{-1}), with its opening located 8 m above the ground and 3 m above the top of the container. The 405 nm channels sampled air via a 1 m long, 1/4 inch PFA tube protruding into the centre of the high-flow inlet. Correction for $ClNO_2$ and N_2O_5 conversion to NO_2 was carried out as described for the PARADE campaign, the removal of the biases was related to reactions by peroxy radicals, and O_3 and NO_x were carried out as described in Sobanski et al. (2016a). The average correction factor for the ΣANs was 1.1, with maximum values of 2. The uncertainty associated with the correction procedure is estimated as ~ 30 % (Thieser et al., 2016). The detection limits were 1.5 and 60 pptv for NO_3 and NO_2 respectively, with uncertainties of 25 % for NO_3 and 6.5 % for NO_2 (Sobanski et al., 2016a).

3.2 NO during PARADE–NOTOMO

During PARADE, NO measurements were made with a modified commercial chemiluminescence detector (CLD 790 SR), the operation of which is described by Li et al. (2015). The detection limit for this instrument is 4 pptv in 2 s, with a total uncertainty of 4 %. This instrument did not participate in NOTOMO and daytime NO mixing ratios were calculated from measurements of NO_2, O_3, and $J(NO_2)$ assuming photo stationary state

$$[NO]_{calc} = J(NO_2)[NO_2]/k_{(NO+O_3)}[O_3], \quad (1)$$

where $J(NO_2)$ is the photolysis frequency of NO_2 (measured using a METCON spectral radiometer) and $k_{(NO+O_3)}$ is the temperature-dependent rate constant for reaction of NO with O_3. This expression ignores the oxidation of NO to NO_2 via e.g. reactions of peroxy radicals and thus overestimates NO. However, this method of estimating NO resulted in satisfactory agreement (within $\approx 20\,\%$) with measurements from the HLNUG for periods when NO was above the detection limit (> 1 ppb) of their instrument. Night-time concentrations of NO during NOTOMO were assumed to be zero, consistent with measurements on many nights during previous campaigns at this site (Crowley et al., 2010; Sobanski et al., 2016b).

3.3 VOC measurements during PARADE

The VOC measurements have already been described by Sobanski et al. (2016b). Briefly, VOCs were measured using two gas chromatographic (GC) instruments (1 data point per hour) with a mass spectrometer (MS) and a flame ionization detector (FID). The GC-MS (biogenic and aromatic hydrocarbons) had a detection limit of around 1 pptv with an uncertainty of 10–15 %. The GC-FID (non-methane hydrocarbons) had detection limits between 1 and 5 pptv, exceptions being ethane, ethene, propene, benzene, and toluene with values of 8, 16, 9, 14, and 48 pptv respectively and a total uncertainty of 10 % (15 % for 1-pentane). The GC measurements for butadiene and pentene were unrealistically high, probably a result of poor separation of trace gases with similar retention times, and are not reported. The VOCs measured during PARADE are listed in Table 1 along with their rate constants, k_{OH+VOC}, for reaction with OH. The associated alkyl nitrate yields, α(OH), are also listed. We also list calculated production rates of ANs (P(ANs)) and O_3 ($P(O_3)$) derived from midday OH levels during PARADE.

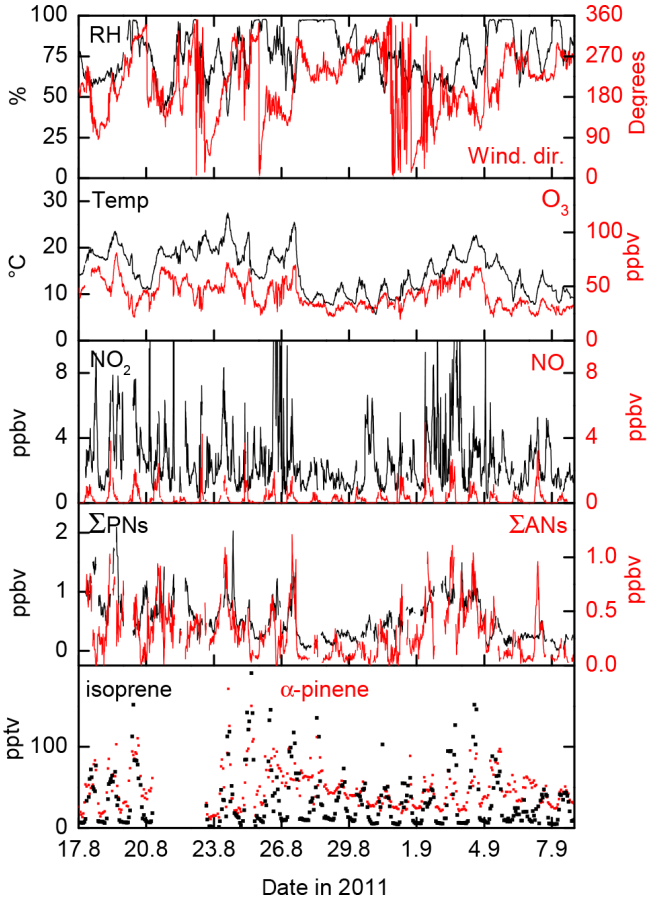

Figure 1. PARADE 2011: time series of relative humidity (RH), wind direction, temperature, and the O_3, NO_2, NO, ΣPN, and ΣAN mixing ratios. The lowest panel shows the mixing ratios of isoprene (black datapoints) and α-pinene (red datapoints).

4 Results and discussion

4.1 NO_x and organic nitrates at the Taunus Observatory

The temperature, humidity, wind direction, O_3, NO, NO_2, ΣPNs, and ΣANs for the PARADE and NOTOMO campaigns are shown in Figs. 1 and 2 respectively. The reactive nitrogen species are plotted at 10 min resolution, and Table 2 summarizes selected minimum, maximum, and mean values for the two datasets. The data provided by the HLNUG are given at 30 min intervals.

During PARADE and NOTOMO, NO_2 varied between ≈ 1 and 15 ppbv, with the highest mixing ratios (during PARADE) associated with air mass originating from the south and from the south-west, corresponding approximately to the urbanized Frankfurt and Wiesbaden–Mainz sectors. The ΣPN mixing ratio varied from below the detection limit to ≈ 3 ppbv during NOTOMO. Low values approaching or below the detection limit were measured during episodes of persistent fog and rainfall. The campaign means for ΣPNs were 505 pptv for PARADE and 677 pptv for NOTOMO. ΣAN mixing ratios varied from below the detection limit to 1.2 ppbv (PARADE maximum), with campaign mean values of 297 pptv for PARADE and 116 pptv for NOTOMO. Figures 1 and 2 show that ΣPNs and ΣANs co-vary at the Taunus Observatory and also show a correlation with O_3 both in terms of their diel profile (see below) and day-to-day variability.

Measurements of individual peroxyacyl nitrates are numerous, especially of PAN, which usually represents $\sim 80\,\%$ of all peroxy nitrates in the lower troposphere (Roberts, 1990; Roberts et al., 1998). This has been shown to also be the case at the Taunus Observatory (Thieser et al. 2016). Our measurements of ΣPNs are in the range of PAN or the sum of individual PAN mixing ratios observed in different urban–suburban locations (Roberts, 1990; Roberts et al., 2007; LaFranchi et al., 2009). Measurements of individual alkyl nitrates are more sparse. Early estimates for the to-

Table 2. Minimum, mean, and maximum values for relative humidity, temperature, ozone, NO, NO_2, and organic nitrates during the PARADE and NOTOMO campaigns.

	PARADE (August–September 2011)			NOTOMO (July 2015)		
Species	Minimum	Maximum	Mean	Minimum	Maximum	Mean
Relative humidity (%)	38	100	77	27	100	70
Temperature (°C)	6	27	15	6	33	17
O_3 (ppbv)	8	81	41	17	150	48
NO_2 (ppbv)	0.3	21	2.7	0.1	15	2
NO (ppbv)	< LOD	5	0.3	0*	3*	0.3*
ΣPNs (ppbv)	< LOD	2	0.5	< LOD	3.2	0.7
ΣANs (ppbv)	< LOD	1.2	0.3	< LOD	0.8	0.1

* Calculated using measurements of NO_2, O_3, and $J(O^1D)$ and assuming photostationary state (see text for details).

tal alkyl nitrate burden at rural locations influenced by urban emissions up to a few hundred parts per trillion per volume were derived by summing the mixing ratio of individually measured alkyl nitrates (C1 up to C8) by gas chromatography technics (Flocke et al., 1991, 1998; Russo et al., 2010; Worton et al., 2010). Recent developments in chemical ionization mass spectrometry have enabled measurement of more complex, multifunctional nitrates of biogenic origin and revealed the occasional presence of parts per billion per volume levels of the sum of measured alkyl nitrates (Beaver et al., 2012). Our measurements of ΣPNs and ΣANs can be more directly compared to those of the University of California at Berkeley, who have developed and applied the technique of thermal dissociation laser-induced fluorescence (TD-LIF) over the last 15 years (Day et al., 2002; Wooldridge et al., 2010; Perring et al., 2013). The mixing ratios of ΣPNs and ΣANs at the Taunus Observatory are comparable to summertime measurements of ΣPNs and ΣANs (0–2 and 0–1 ppbv respectively) at forested sites in California (Day et al., 2003, 2008; Murphy et al., 2006).

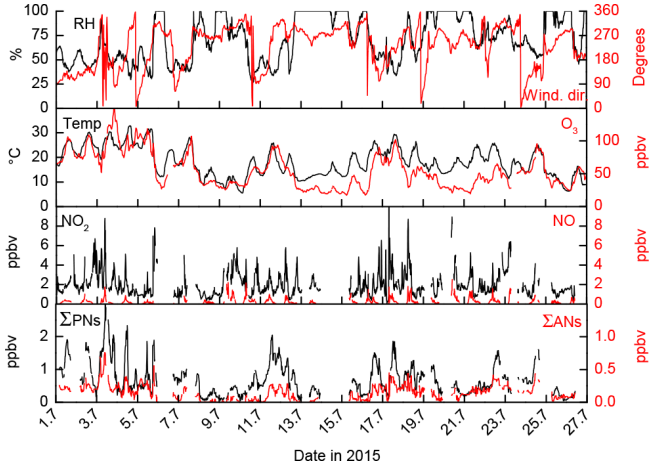

Figure 2. NOTOMO 2015: time series of relative humidity (RH), wind direction, temperature, and the mixing ratios of O_3, NO_2, NO, ΣPNs, and ΣANs. The NO mixing ratios were calculated assuming photostationary state as described in the text.

4.2 Sequestering of NO_x as organic nitrates

In this section, we examine how much NO_x is sequestered as organic nitrates at this site. As HNO_3 was not measured during either campaign, we cannot examine the relative efficiency of NO_x conversion to organic nitrates compared to inorganic HNO_3, though we expect the former to dominate in air masses in the continental boundary layer that have significant anthropogenic or biogenic emissions of hydrocarbons (Day et al., 2008).

Figure 3 shows the fraction, $f(NO_x)$, of NO_x sequestered as organic nitrates ($f(NO_x)$ = ([ΣPNs] + [ΣANs]) / ([ΣPNs] + [ΣANs] + [NO_x])), plotted versus NO_x and colour coded for temperature. It clearly shows that $f(NO_x)$ is higher at low NO_x and could be as high as 0.75 in air masses containing less than 2 ppbv of NO_x. The lowest values of $f(NO_x)$ measured (< 0.08) were associated with levels of NO_x in excess of 10 ppbv. At this location, high values of NO_2 are associated with freshly emitted anthropogenic pollution originating from the nearby urban centres. The high values of $f(NO_x)$ during periods of low NO_x are the result of efficient conversion of NO_x to longer-lived organic nitrates in photochemically aged air masses at this site. Furthermore, the temperature dependence indicates that organic nitrate formation is not limited by NO_x. For a given level of NO_x, $f(NO_x)$ is larger when temperatures are higher, reflecting stronger biogenic emissions and more intense photochemical activity and thus conversion rates of NO_x to organic nitrates (Olszyna et al., 1994; Day et al., 2008). However, note that low temperatures also increase the rate of transfer of soluble organic nitrates to the aerosol phase, which acts on $f(NO_x)$ in the same direction.

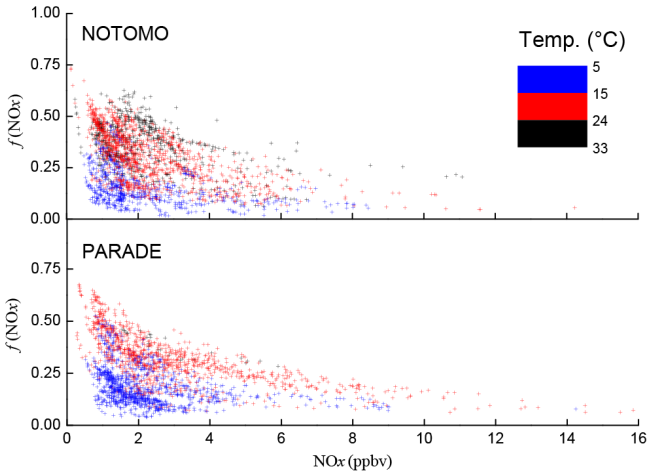

Figure 3. The fraction of NO_x sequestered as organic nitrates $f(NO_x) = [\Sigma PNs] + [\Sigma ANs] / ([\Sigma PNs] + [\Sigma ANs] + [NO_x])$ as a function of NO_x for the NOTOMO and PARADE campaigns, both colour coded for temperature.

4.3 Diel profiles: photochemical and meteorological influences

Figure 4 shows the mean diel profiles of $J(O^1D)$, O_3, temperature, humidity, NO_2, ΣPNs, and ΣANs for the PARADE (dashed lines) and NOTOMO (solid lines) campaigns. A number of factors, including highly variable (temporal and spatial) local emissions, irradiance, wind direction, and the complex topography at the site, all impose their influence on the diel profiles measured for the organic nitrates.

The campaign-averaged daily maxima in global radiation, temperature, and O_3 mixing ratio were higher during NOTOMO, indicating on average warmer, sunnier, and drier conditions in July 2015. Lower average levels of NO_2 were measured during NOTOMO. The mean PARADE NO_2 profile shows two maxima during the day (at $\sim$10:00 UTC and $\sim$19:00 UTC), which approximately correspond to local rush hour traffic increases during the working week. These NO_2 maxima are less clearly defined but still apparent in the averaged diel profiles in NOTOMO. A close inspection of the NOTOMO data revealed that the days can be divided into two types, 7 of which display the rush hour peaks in NO_2 and 23 that do not.

As illustrated in Fig. 5, rush-hour-influenced days were associated with higher temperatures and levels of O_3 and a local wind direction that has a large daytime component from the south, whereas the other days were cooler, had less O_3, and the local wind had a dominant westerly component. Air masses arriving from the southerly sectors are influenced by rush hour traffic from the nearby urban centres, whereas those arriving from the west are cleaner, with an Atlantic influence and more distant emissions of NO_x. Upslope winds, resulting from enhanced rates of heating of the mountainside during the warmer periods, can also play

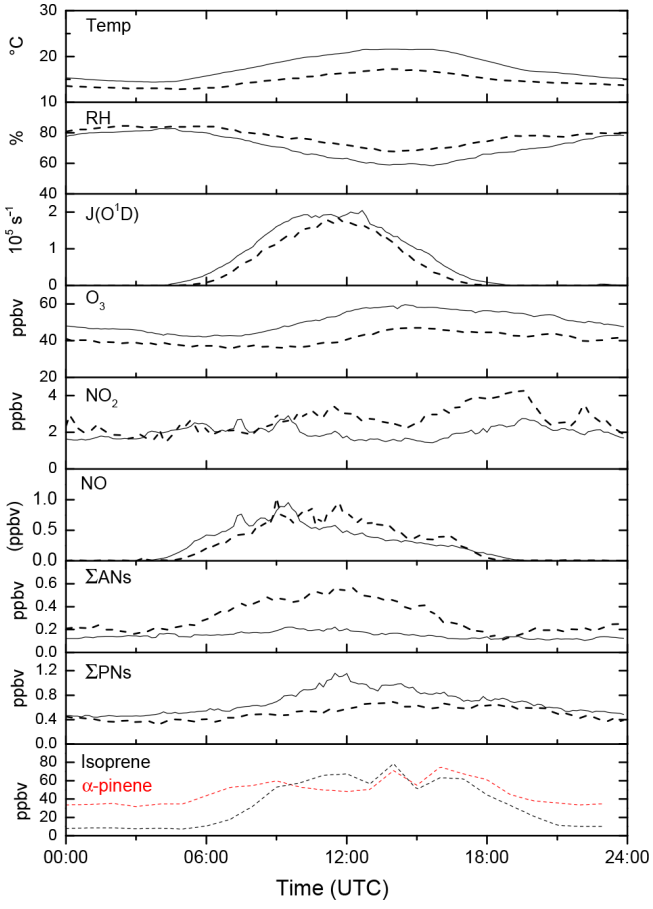

Figure 4. Mean diel profiles during PARADE (dashed lines) and NOTOMO (solid lines) of $J(O^1D)$, O_3, temperature, NO_2, ΣPNs, and ΣANs. Isoprene and α-pinene were measured only during PARADE.

a role in enhancing rates of transport of NO_x and photochemically produced trace gases to the site compared to the cooler, cloudier days under the influence of westerly winds. The mean ΣPN profiles during both campaigns (Fig. 4) indicate an increase in mixing ratio starting at about sunrise, with a broad daily maxima between $\approx$12:00 and 14:00 UTC for NOTOMO. The mean daily maximum for NOTOMO was about 1.2 ppbv, a factor of 2 or more than for PARADE. In contrast, during PARADE the mean daily maximum of ΣANs ($\approx$0.6 ppbv) was about a factor of 3 larger than during NOTOMO. The ratio of the mean daily maximum of ANs to PNs ($[ANs]_{max}/[PNs]_{max}$) was thus very different for the two campaigns, with values of close to 1 for PARADE and $\approx$0.2 for NOTOMO.

A number of factors influence the relative concentrations of PNs and ANs. In general, higher temperatures are the result of higher levels of insolation and are thus usually related to higher O_3 concentrations and rates of photochemical processing of VOCs. This should lead to higher concentrations of both PNs and ANs. Higher levels of insolation will lead to

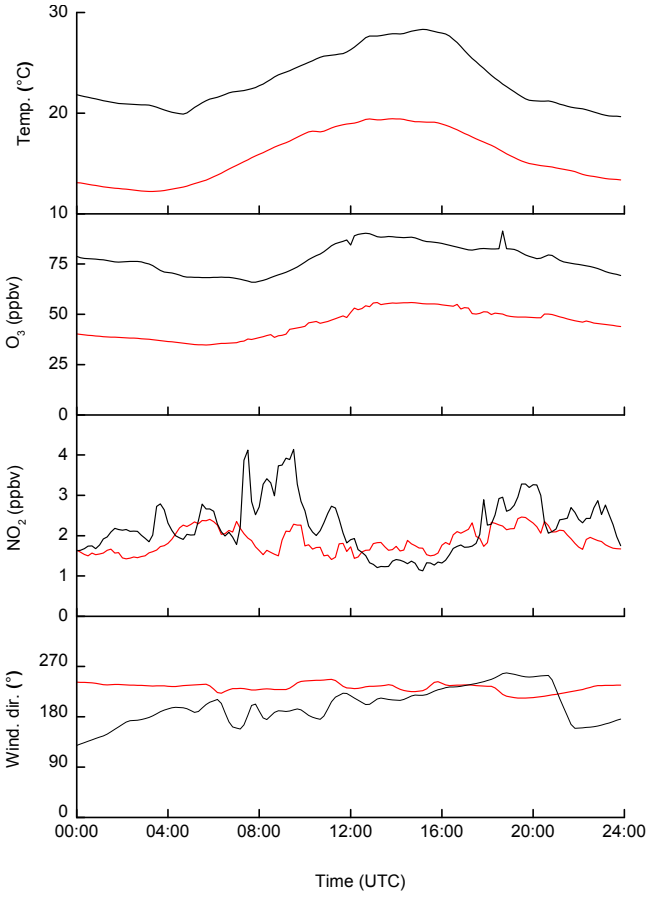

Figure 5. Mean daily profiles of O_3, temperature, NO_2, and wind direction for the NOTOMO campaign separated into days with a clear influence from local rush hour traffic (black). The rest are shown in red.

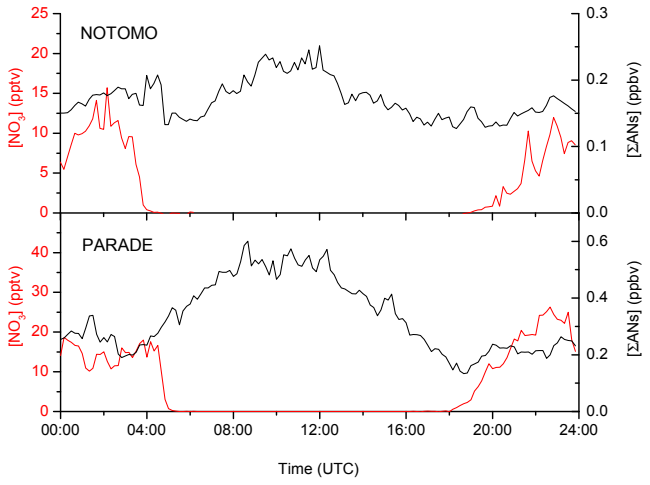

Figure 6. Mean daily profiles of NO_3 (red) and ΣANs (black) for the NOTOMO (top) and PARADE campaigns (bottom) for relative humidity $< 90\,\%$.

higher NO-to-NO_2 ratios (noon NO_2-to-NO ratios were 4.0 (PARADE) and 3.8 (NOTOMO) and, given sufficient NO, elevated temperatures will reduce the lifetimes of PNs. Altogether, higher temperatures and more insolation favour AN production over PN production during the two campaigns. This is essentially the opposite to what we observe and we conclude that other factors, including the mechanism of organic nitrate production from oxidation of different VOC types and rates of loss of the organic nitrates play a major role in controlling the relative abundance of ANs and PNs at this site (see below).

4.4 Daytime and night-time production of alkyl nitrates

During PARADE, the diel profiles of ΣANs show a maximum around 12:00 UTC, similar to the maximum in global radiation that drives primary OH formation, VOC oxidation, and peroxy radical production rates. However, as indicated in Sect. 1, ANs can also be formed by the reaction of NO_3 radicals with biogenically emitted VOCs, which can impact their diel profile. Figure 6 shows median profiles of ΣANs obtained by filtering out periods with fog and rain at the site at which NO_3 would have been absent due to the rapid, heterogeneous scavenging of N_2O_5, with which it is in thermal equilibrium. We also plot the mean profiles of NO_3 during these nights (representing 16 "dry" nights for PARADE and 13 dry nights for NOTOMO). The most notable change compared to Fig. 4 is the increase in ΣANs during the night. For the NOTOMO campaign, the night-time ΣANs represent $\sim 60\,\%$ of the daytime value, while for PARADE this is $\sim 35\,\%$. As described in Thieser et al. (2016) and Sobanski et al. (2016a), the potential artefact caused by thermal decomposition of either $ClNO_2$ or N_2O_5 (present during some nights in amounts of up to several hundred parts per trillion per volume) in the hot inlets of the TD-CRDs was accounted for by the simultaneous measurement of both of these trace gases and therefore does not contribute to the night-time signal we ascribe to ANs.

We now explore potential meteorological and chemical contributions to the night-time increases in ΣANs. Sobanski et al. (2016b) report occasionally extended NO_3 lifetimes (> 1000 s) at this site that result from sampling from a low-lying residual layer. Compared to the lowest levels, the residual layer is likely to contain higher levels of photochemically generated trace gases (e.g. ANs), which would otherwise be lost by deposition. During PARADE and NOTOMO, the majority of nights were, however, characterized by NO_3 lifetimes of the order of minutes or less, which indicates that NO_3 is removed by reaction with VOCs, presumably mainly reactive terpenoids with double bonds. Those nights (altogether four) with long NO_3 lifetimes during PARADE were excluded for calculating the NO_3 and ΣAN profiles in Fig. 6.

The reaction between NO_3 and unsaturated VOCs is known to produce alkyl nitrates with a higher yield than the

daytime pathway through OH-induced oxidation of VOCs and is a plausible explanation of the night-time maxima in ΣANs shown in Fig. 6. In order to assess this, we calculated the night-time and daytime maxima and the production of alkyl nitrates during PARADE as described below.

4.4.1 Night-time generation of ANs in PARADE via NO_3 reactions

To estimate the night-time production of ANs, we consider the reaction between NO_2 and O_3 to be the only NO_3 precursor. Of the measured VOCs, isoprene, α-pinene, myrcene, and limonene account for > 95 % of the NO_3 reactivity and have substantial yields of ANs. The mean night-time mixing ratios for these four compounds during PARADE (excluding data where RH > 92 %) are listed in Table 3 along with the corresponding NO_3 reaction rate coefficients (k) and the alkyl nitrate yields (α) as reported by the IUPAC panel (IUPAC, 2016). The effective alkyl nitrate yield for this VOC mixture can be calculated from the relative flux of NO_3 reacting with each biogenically emitted VOC (BVOC; depending on the BVOC mixing ratio and rate coefficient) and the alkyl nitrate yield for each individual BVOC. Note that in the absence of laboratory investigations, the alkyl nitrate yield from NO_3+ myrcene is simply estimated as 50 ± 30 %, in line with other terpenes (IUPAC, 2016). The final averaged yield of alkyl nitrate is $\alpha(NO_3) = (0.41 \pm 0.31)$. The uncertainty we quote is propagated from uncertainty in the rate coefficient and the individual alkyl nitrate yields as reported by IUPAC and also the standard deviation of the mean concentration of the BVOC during the campaign. Clearly, given the large variability in night-time BVOC at this site, uncertainty associated with alkyl nitrate yields and the assumption that all BVOCs with significant reactivity for NO_3 were measured, this campaign average value of $\alpha(NO_3)$ should be considered only as a rough indicator. Assuming that each NO_3 generated reacts rapidly with a BVOC, the night-time production rate of ANs is then given by

$$P(\Sigma\mathrm{ANs})_{\mathrm{night}} = \alpha(\mathrm{NO_3}) k_{(\mathrm{NO_2+O_3})} [\mathrm{NO_2}][\mathrm{O_3}]. \quad (2)$$

Taking the mean night-time mixing ratios of NO_2 (2.7 ± 2.1 ppbv) and O_3 (45 ± 11 ppbv) over the same time period, using the temperature-dependent rate coefficient for the reaction between NO_2 and O_3 ($1.4 \times 10^{-13} \exp(-2470/T)$ cm^3 molecule^{-1} s^{-1}) we calculate the production rate of ANs (Eq. 2) to be $P(\Sigma\mathrm{ANs})_{\mathrm{night}} \approx 90$ pptv h^{-1}. This analysis implicitly assumes that indirect loss of NO_3 via the heterogeneous loss of N_2O_5 is insignificant compared to direct loss via reaction with BVOCs. This is expected for a forested region in summer and has been shown to be the case for the Taunus Observatory (Crowley et al., 2010; Sobanski et al., 2016b), where, except for a few occasions when the residual layer is sampled, the NO_3 lifetime with respect to gas-phase reactions with BVOCs is too short for indirect, heterogeneous loss to compete unless the mountain site is in fog.

Table 3. Mean night-time BVOC mixing ratios during PARADE.

BVOC	Mean ± SD[1]	$k^2_{\mathrm{NO_3+VOC}}$	Relative flux	$\alpha_{\mathrm{NO_3+VOC}}$
limonene	23.9 ± 12	120 ± 36	0.40 ± 0.23	0.5 ± 0.2
myrcene	19.7 ± 11.8	110 ± 33	0.30 ± 0.20	0.5 ± 0.3[3]
α-pinene	33.1 ± 14.1	62 ± 16	0.29 ± 0.14	0.17 ± 0.3
isoprene	14.0 ± 14.3	6.5 ± 2.6	0.01 ± 0.01	0.75 ± 0.15

[1] Mixing ratios in parts per trillion per volume. [2] Rate constants (298 K) in 10^{-13} cm^3 molecule^{-1} s^{-1}. Rate constants (and associated uncertainty) and organic nitrate yields (with spread of measurements) were taken from IUPAC (IUPAC, 2016). [3] In the absence of experimental data, this value is an estimate with expanded error limits.

Given the large uncertainty associated with $\alpha(NO_3)$, and also the variability in NO_2 and O_3, this average value can be considered consistent with the increase in ANs observed in the 2 h following sunset during either the PARADE or NOTOMO campaign.

4.4.2 Daytime generation of ANs in PARADE via OH reactions

To calculate the daytime production of ANs from OH-initiated degradation of VOCs, it is necessary to know the OH concentration. During the PARADE campaign, OH was measured on only a few days that did not cover those used to derive our diel profiles. Following Bonn et al. (2014), who performed a detailed analysis of OH measurements and their correlation with $J(\mathrm{O^1D})$ during PARADE, we calculate $[\mathrm{OH}] = 1.8 \times 10^{11} \times J(\mathrm{O^1D}) \approx 3 \times 10^6$ molecule cm^{-3} for the mean OH between 11:00 and 13:00 UTC. Bonn et al. (2014) report a maximum uncertainty of a factor 2 for OH derived in this manner. For an approximate estimate of daytime AN production, we take the campaign mean mixing ratios of each VOC between 11:00 and 13:00 UTC as listed in Table 1. Based on the individual rate coefficients, alkyl nitrate yields, and mean noon concentrations of the VOCs measured (also listed in Table 1), and using Eq. (3),

$$P(\Sigma\mathrm{ANs})_{\mathrm{day}} = \Sigma_i \left(\alpha_i(\mathrm{OH}) k_{\mathrm{OH+RH}_i} [\mathrm{OH}][\mathrm{RH}_i]\right), \quad (3)$$

we obtain a noon AN production rate of $P(\Sigma\mathrm{ANs})_{\mathrm{day}} \approx 70^{+70}_{-35}$ pptv h^{-1}, where the reported uncertainty is due only to the uncertainty in OH concentrations. As illustrated in Table 1, ∼ 80 % of the total noon ΣAN production rate is accounted for by the four biogenic VOCs measured: limonene, myrcene, α-pinene, and isoprene. Given that the concentrations of these short-lived biogenics are expected to be variable due to the spatial inhomogeneity of emission sources and their dependence on temperature and light levels, the use of campaign averages can provide only a rough indicator of AN production rates. In addition, there is considerable uncertainty associated with the AN yields of the biogenics, which in the absence of measurements, partially stem from structure–reactivity relationships (Perring et al., 2013). The

largest uncertainty is, however, related to the assumption that the reactions of OH are accounted for by the VOCs measured. In forested regions "missing" OH reactivity has been frequently reported (Nölscher et al., 2012, 2013), indicating unknown sinks for OH with organic trace gases, which can account for up to 80 % of the observed reactivity. In the case of missing reactivity, the ΣAN yields calculated via Eq. (3) are lower limits. Moreover, this expression also neglects the formation of peroxy radicals from the Cl-atom-initiated oxidation of VOCs, which may also react with NO to form ANs. As $ClNO_2$ was observed at elevated concentrations on some days during PARADE (Phillips et al., 2012), its main influence on oxidation processes is in the early morning, when OH levels are comparably low. Despite these uncertainties, the calculations above indicate that the value of $P(\Sigma ANs)_{day}$ thus obtained is comparable with the estimated night-time production, which is consistent with the conclusions of Fry et al. (2013) also made at a forested site with urban influence.

From the discussion above, it is apparent that the relative rates of noon- and night-time generation of ΣANs depend on the relative levels of OH and NO_3 (a factor ≈ 200 in favour of NO_3), the yields of ANs (generally larger for NO_3), and the rate constant for reaction of OH with VOCs. The large night-time production rate from NO_3 degradation of VOCs in this forested environment is mainly a consequence of the selective reactivity of NO_3 towards terpenes, which have large AN yields.

Although we calculate similar production rates of ΣANs during the night when NO_3 is present, the daytime maximum in the ΣAN mixing ratio is significantly larger, which has a number of likely causes. The first is related to missing OH reactivity, which, depending on the hydrocarbons involved, could potentially increase the OH-initiated rate of formation of ΣAN yield by large factors. For example, if the hydrocarbons we measured would account for only 50 % of the OH reactivity and the missing ones were biogenic in nature (i.e. terpenoids with large AN yields) we could expect an increase of more than a factor of 2 in calculated $P(\Sigma ANs)_{day}$. A further potential cause for larger daytime ΣAN mixing ratios is a reduced loss of daytime ΣANs with respect to chemical and depositional loss and condensation. This being a consequence of the different chemical composition and volatility of the ANs generated from NO_3- compared to OH-initiated oxidation. It is well established in chamber studies that the NO_3-induced oxidation of biogenics leads to highly functionalized ANs that partition largely to the aerosol phase and that the NO_3 oxidation of biogenic VOCs can lead to appreciable organonitrate content in atmospheric particulate matter (Fry et al., 2011, 2014; Boyd et al., 2015). Ambient measurements of aerosol composition show that night-time-generated organic nitrates formed in NO_3+ BVOC reactions are efficiently transferred to the condensed phase (Rollins et al., 2012; Fry et al., 2013; Xu et al., 2015; Kiendler-Scharr et al., 2016), which is confirmed by modelled vapour pressures of the OH- and NO_3-initiated organic nitrate products from BVOC oxidation, the latter being substantially lower (Fry et al., 2013).

Table 3 shows that (of the BVOCs measured) limonene accounts for 40 % of the NO_3 loss rate, myrcene 30 %, and α-pinene 29 %. Studies of the reaction between α-pinene and NO_3 show that the yield of secondary organic aerosol (SOA) is less than 10 % (Hallquist et al., 1999; Perraud et al., 2010; Fry et al., 2014; Nah et al., 2016), with reports of the alkyl nitrates formed being exclusively in the gas phase (Fry et al., 2014). This contrasts strongly with the situation for limonene, where SOA yields of up to ≈ 60 % have been reported, with more than 80 % of the alkyl nitrates formed being in the aerosol phase. There is no experimental data on SOA yields in the reaction between NO_3 and myrcene or on the gas-aerosol partitioning of the alkyl nitrates formed. Recent experiments on β-pinene (Boyd et al., 2015) have shown that the SOA yield is neither strongly dependent on the relative concentrations of HO_x and NO_x, which determine the nature of the end products formed, nor on the relative humidity or seed aerosol used. If we make the broad assumptions that (1) the SOA yield from myrcene is the same as limonene and (2) the fraction of ANs in the condensed phase is comparable to that found for limonene, we calculate that > 60 % of the alkyl nitrates formed at night at this site will be present in the aerosol phase and thus not detected by our instrument. In other words, we would expect Eq. (3) to yield production rates of ΣANs that exceed those derived from gas-phase ΣAN measurements by a factor between 2 and 3.

We conclude that the apparent lower lifetime of night-time-generated ΣANs is thus likely to be the result of an increased fraction of low-volatility ANs formed from terpenes initially reacting with NO_3 compared to OH-initiated oxidation, leading to a larger relative rate of SOA formation and partitioning of ANs to the condensed phase. Fry et al. (2013) have shown that, at an urban–forested site in Colorado, the peak in particle-phase organic nitrates occurs at night-time. The condensed-phase ANs can undergo hydrolysis to HNO_3 (over a period of a few hours; B. H. Lee et al., 2016) and thus irreversible loss from the gas phase, the latter enhanced by the lower temperatures and higher relative humidities encountered at night-time (Hallquist et al., 2009; A. K. Y. Lee et al., 2016).

4.5 Effective yield of ANs from correlation between ΣANs and O_3

A positive correlation between organic nitrates and O_3 has been observed (Kourtidis et al., 1993; Williams et al., 1997; Roberts et al., 1998; Schrimpf et al., 1998; Day et al., 2003) and is due to the common production pathways of these trace gases. In rural and semi-rural locations, the build-up of O_3 during the day is related to the NO_x-catalysed photo-oxidation of VOCs, including the reaction of organic peroxy radicals with NO_x. These processes also dominate the daytime production of organic nitrates. As discussed in Sect. 1,

alkyl nitrates are produced via a minor branch of the reaction between NO and organic peroxy radical, while the majority of reactive collisions result in the formation of NO_2 and (via its photolysis) the formation of O_3 (Reactions R4 to R5). Laboratory experiments have shown that the branching ratio to ANs is strongly dependent on the identity of the peroxy radical and also varies with temperature and pressure (Perring et al., 2013). As we measure total alkyl nitrates, the effective branching ratio is determined by the particular VOC mixture encountered. Following the methodology developed by the Berkeley group (Day et al., 2003; Rosen et al., 2004), the production rate of O_3 (P_{O_3}) is given by Eq. (4).

$$P_{O_3} = \Sigma_i \left(\gamma_i (1-\alpha_i(\mathrm{OH}))k_{\mathrm{OH+RH}_i}[\mathrm{OH}][\mathrm{RH}_i]\right), \quad (4)$$

where α(OH) is the branching ratio to nitrate formation in the reaction between the OH-generated organic peroxy radical and NO, and γ is the number of O_3 produced per VOC oxidized, which can be between 1 and 3 but is equal to 2 for many atmospherically relevant VOCs, given sufficient NO (see Table 1) (Rosen et al., 2004). This can be combined with Eq. (3) to give

$$\frac{\Delta O_3}{\Delta \Sigma \mathrm{ANs}} = \frac{\int (P_{O_3} - L_{O_3} + E_{O_3})\mathrm{d}t}{\int (P_{\Sigma \mathrm{ANs}} - L_{\Sigma \mathrm{ANs}} + E_{\Sigma \mathrm{ANs}})\,\mathrm{d}t} \quad (5)$$

$$\frac{\Delta O_3}{\Delta \Sigma \mathrm{ANs}} = \frac{2(1-\alpha)}{\alpha} \approx \frac{2}{\alpha}, \quad (6)$$

in which L represents loss terms (chemical and deposition) and E represents entrainment. The ratio of O_3 to ΣANs after the OH oxidation of a VOC mixture has proceeded for a certain time, dt, is given by Eq. (5). At sufficiently high levels of OH, VOCs, and NO, the photochemical production terms can be assumed to be larger than the loss or entrainment terms and Eq. (5) simplifies to Eq. (6). In principal, a plot of O_3 versus ΣANs should then yield a straight line, with a slope that is proportional to an average value of the branching ratio to ANs. The average values of α(OH) we calculate using the measurement of ΣANs and O_3 is designated $\alpha(\mathrm{OH})_{\mathrm{av}}^{\Sigma \mathrm{ANs}}$. Alternatively, an average value of α(OH) can be calculated from measurement of the VOCs that react with OH, their rate constant and the individual yield of alkyl nitrate from each reaction and the O_3 yield, which we then designate $\alpha(\mathrm{OH})_{\mathrm{av}}^{\mathrm{VOC}_i}$.

For both the PARADE and NOTOMO campaigns, we analysed the mixing ratios of ΣANs and O_3 between 11:00 and 13:00 UTC (around the peak in $J(\mathrm{O}(^1\mathrm{D}))$ and thus OH levels) to calculate $\alpha(\mathrm{OH})_{\mathrm{av}}^{\Sigma \mathrm{ANs}}$. The results, displayed in Fig. 7, indicate a value of $\alpha(\mathrm{OH})_{\mathrm{av}}^{\Sigma \mathrm{ANs}}$ (PARADE) = $7.2 \pm 0.5\,\%$ ($R^2 = 0.49$). In this analysis, the intercept, 28.6 ± 1.2 ppbv, may be thought of as the average background level of O_3. In the NOTOMO dataset, the yield of ΣANs is low and the data are very scattered, with a poor correlation coefficient; hence, no fit was carried out and we simply plot (black lines) two lines, which encompass the whole dataset with corresponding values of $\alpha(\mathrm{OH})_{\mathrm{av}}^{\Sigma \mathrm{ANs}}$ equal to

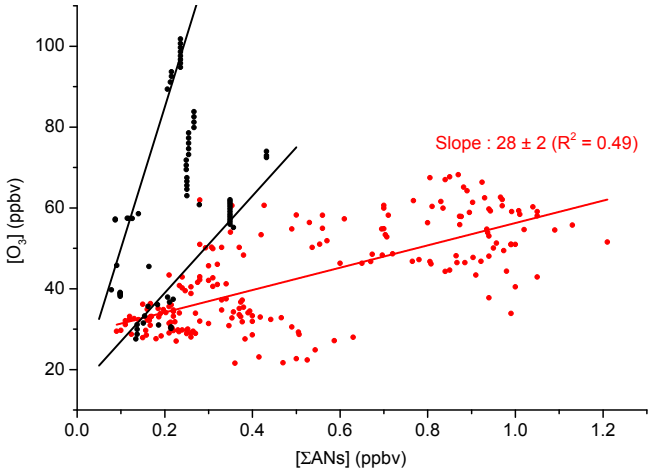

Figure 7. O_3 versus ΣANs measured between 11:00 and 13:00 UTC during PARADE (red data points) and NOTOMO (black data points). The red line is the best fit for PARADE. For NOTOMO the black line is chosen to encompass all possible values of α, assuming a background O_3 level of 15 ppbv. The apparent, poor resolution in the NOTOMO data is due to the low yield and the iterative correction procedure as described in the text.

0.5 and 1.7 %, which is significantly lower than that derived for PARADE. For NOTOMO, in which low mixing ratios of ΣANs were encountered, the vertical grouping of the data apparent in Fig. 7 (i.e. low resolution in concentration) is a result of the corrective procedure for extracting mixing ratios from raw data obtained in the hot and cold inlets, which involves iterative numerical simulation that converges when 1 % agreement between observation and simulation is achieved. The average correction factor for ΣANs during NOTOMO was 1.1 (Sobanski et al., 2016a) and, based on a series of laboratory experiments, the NO_x-dependent uncertainty associated with this factor is expected to be less than 50 %.

For the PARADE campaign, during which VOCs were measured, we derive a value of $\alpha(\mathrm{OH})_{\mathrm{av}}^{\mathrm{VOC}_i} = 6.1\,\%$ for the same period around noon (UTC), which is consistent with the value of $7.2 \pm 0.5\,\%$ derived from measured ΣANs and O_3. Irrespective of the method used to derive the branching ratio to ΣAN formation, the high values obtained reflect the fact that a significant fraction of OH reactivity is due to biogenic VOCs (especially terpenoids, including isoprene, monoterpenes, and sesquiterpenes) that have large yields of alkyl nitrates. To emphasise the different efficiency of AN production and VOCs of biogenic origin (BVOC) and anthropogenic origin (AVOC), Table 1 is separated into biogenic and anthropogenic VOCs. From the separate summed P(ANs) and $P(O_3)$, we calculated the effective value of $\alpha(\mathrm{OH})_{\mathrm{av}}^{\mathrm{VOC}_i}$ that would have been obtained considering each class of VOC individually. The values thus obtained are $\alpha(\mathrm{OH})_{\mathrm{av}}^{\mathrm{BVOC}_i} = 17.3\,\%$ and $\alpha(\mathrm{OH})_{\mathrm{av}}^{\mathrm{AVOCi}} = 1.4\,\%$. Note that

for this particular hydrocarbon mixture, the O_3 production rates are much larger for the AVOCs (~ 1000 compared to ~ 400 for the BVOCs).

To some extent, the agreement may be fortuitous since both methods to derive $\alpha(\mathrm{OH})_{\mathrm{av}}$ involve assumptions that may only be partially applicable. The value of $\alpha(\mathrm{OH})_{\mathrm{av}}^{\mathrm{VOC}_i}$ calculated using individual VOC measurements and their respective alkyl nitrate yields is associated with a rather large uncertainty as it assumes that all VOCs with which OH reacts were actually measured during the campaign and that their alkyl nitrate yields are well known. For example, the products of isoprene oxidation, methyl vinyl ketone, and methacrolein have high reported $\alpha(\mathrm{OH})$ values (Paulot et al., 2009) and high rate constants for reaction with OH, which, if taken into account, would increase the value of $\alpha(\mathrm{OH})$. Regarding the individual nitrate yields, some values used to calculate the average (see Table 1) are not precisely determined in the literature, while others are estimated. For example, the most recent measurements of the yield of alkyl nitrates formed in the reaction of OH with isoprene in the presence of NO_x (one of the best-studied reaction systems) ranges from 6 to 13 % (Xiong et al., 2015) and remains a source of uncertainty (Perring et al., 2013).

Our calculation of $\alpha(\mathrm{OH})_{\mathrm{av}}^{\mathrm{VOC}_i}$ will also be biased if, for example, local emissions of biogenics are larger than those averaged over the time period over which O_3 and ANs were formed. Likewise, neglecting terms for entrainment and loss of ANs and O_3 will introduce a variable bias into calculations of $\alpha(\mathrm{OH})_{\mathrm{av}}^{\Sigma\mathrm{ANs}}$. The rapid loss of multifunctional ANs from terpene oxidation will bias the analysis to low vales of $\alpha(NO_3)$ (Fry et al., 2013). In the absence of information regarding the condensation rate or efficiency of deposition of a mixture of multifunctional nitrates or O_3 to the topographically complex terrain at the Taunus Observatory, a more detailed analysis is not warranted. The analysis does, however, make comparison with similar analyses for ΣAN measurements possible, and our derived values of $\alpha(\mathrm{OH})_{\mathrm{av}}^{\Sigma\mathrm{ANs}}$ are consistent with those summarized by Perring et al. (2013) obtained both by observation of ΣANs ($7.1\,\% > \alpha(\mathrm{OH})_{\mathrm{av}}^{\Sigma\mathrm{ANs}} > 0.8\,\%$) and calculated from VOC measurements ($10.6\,\% > \alpha(\mathrm{OH})_{\mathrm{av}}^{\mathrm{VOC}_i} > 0.1\,\%$) in various rural and urban locations. A similar analysis by Fry et al. (2013) of ΣAN and O_3 mixing ratios obtained during summer at a forest site with urban influence resulted in a value of $\alpha(\mathrm{OH})_{\mathrm{av}}^{\Sigma\mathrm{ANs}} = 2.9\,\%$, intermediate between the value presented here for the PARADE and NOTOMO campaigns.

4.5.1 Inter-annual and seasonal differences in α(OH), PARADE versus NOTOMO

The difference in $\alpha(\mathrm{OH})_{\mathrm{av}}^{\Sigma\mathrm{ANs}}$ between the July 2011 PARADE campaign ($7.2 \pm 0.5\,\%$) and the August–September 2015 NOTOMO campaign ($< 2\,\%$) is significant and cannot be explained by the uncertainty in the measurements of O_3 or ΣANs (see Sect. 3.1).

There are a number of potential causes for the apparent difference in $\alpha(\mathrm{OH})_{\mathrm{av}}^{\Sigma\mathrm{ANs}}$ between the two campaigns. We first consider the validity of the assumption (Eq. 6) that losses and/or entrainment of ANs and O_3 can be neglected. Xiong et al. (2015) have shown that losses of isoprene-derived nitrates (IN) due to reaction with OH (Lee et al., 2014) and photolysis can be rapid and can start to deplete IN before photochemical production maximizes at the peak of the daytime OH profile. They also indicate that early morning entrainment of IN from the residual layer (where predawn AN mixing ratios may be a factor of 10 larger) can influence its diel profile. This may be particularly relevant for our mountain site, where influence from the free troposphere can be significant. Along with photochemical degradation, dry deposition–hydrolysis can contribute to the alkyl nitrate sink, especially for those derived from biogenic VOCs (Jacobs et al., 2014; Rindelaub et al., 2015). Xiong et al. (2015), report efficient wet and dry deposition of nitrates derived from isoprene with significantly lower mixing ratios measured in conditions of reduced photochemical reactivity–rain. The restriction of the analysis period to close to the maximum of the OH profile should reduce any bias introduced by the assumptions inherent to Eq. (6), but will not remove it totally. As the lifetime with respect to chemical loss–deposition of alkyl nitrates derived from biogenic VOCs is expected to be shorter than that of O_3, the sampling of progressively aged air masses will bias $\alpha(\mathrm{OH})_{\mathrm{av}}^{\Sigma\mathrm{ANs}}$ to low values when calculated from O_3/ΣAN correlations. A low value of $\alpha(\mathrm{OH})_{\mathrm{av}}^{\Sigma\mathrm{ANs}}$ during NOTOMO could conceivably be the result of sampling on average older air masses than during PARADE. The lower NO_x levels in NOTOMO would support this contention, though in the absence of NO_y measurements, this is not conclusive.

A further, related explanation for low values of $\alpha(\mathrm{OH})_{\mathrm{av}}^{\Sigma\mathrm{ANs}}$ during NOTOMO is that the average lifetime of ΣANs was shorter than during PARADE, due to chemically distinct ANs being generated, for example, resulting from a different hydrocarbon mix present during the campaigns. As no BVOC measurements were taken during NOTOMO, we can only speculate on potential reasons for this. We first note that the campaigns were in different seasons and propose that the mountainside vegetation was in different (seasonal) growth phases since NOTOMO (2015) took place during July and was characterized by recurrent damp and foggy conditions, whereas the PARADE campaign (2011) took place later in the year (mid-August to mid-September) during the transition from summer to autumn. The plant-physiology-controlled BVOC emissions depend not only on the temperature and insolation during the two campaigns, which were comparable, but also on the weather (temperature, rainfall, etc.) during the preceding months, which displays a large inter-annual variability at this mountain site. For example, a switch from α-pinene-dominant to β-pinene- or limonene-dominant emissions from the mixed vegetation

could influence not only the ΣAN production rate (there is considerable uncertainty associated with the AN yields; see above) but also the degree to which the ANs are transferred to the particle phase as evidenced by the different yields of secondary organic aerosol formed in these systems (Mutzel et al., 2016). Measurements of OH reactivity at this site in 2011 indicate seasonal differences in the production and emission of BVOCs and suggest that unmeasured primary biogenic emissions contribute significantly to the observed OH reactivity, especially in late summer (PARADE) (Nölscher et al., 2013).

Given the mixed forest–urban location, the hydrocarbon mixture can also be influenced by different average contributions from anthropogenic emissions. An increase in the relative abundance of anthropogenic to biogenic VOCs during NOTOMO would decrease the value of $\alpha(\mathrm{OH})_{\mathrm{av}}^{\Sigma \mathrm{ANs}}$ (see above) and thus reduce the production rate of ΣANs. If a substantial anthropogenic contribution to the VOC mixture was indeed present during NOTOMO, a further reduction in the apparent NOTOMO yield of ANs compared to PARADE could result from increased rates of deposition of the ANs of anthropogenic origin, which are smaller and have more oxidized functional groups per carbon and should thus be more hydroscopic (Fry et al., 2013).

5 Conclusions

By measuring total organic nitrates NO, NO_2, and NO_3, we have shown that a significant fraction (up to 75 %) of NO_x is sequestered as gas-phase organic nitrates at this forested site with urban influence. During the August–September 2011 PARADE campaign, ΣANs and ΣPNs were measured in similar concentrations, whereas in NOTOMO (July 2015) formation of ΣANs was weaker. The difference between the years–seasons may be due to several factors, including varied overall rates of BVOC emission and BVOC speciation during the two campaigns and also breakdown of assumptions used to calculate the effective ΣAN yield. Based on an estimate of the OH concentration and the NO_3-production term, we show that both night-time (NO_3 initiated) and daytime (OH initiated) chemistry contributes to the formation of ANs, which is reflected in their diel profile. Daytime ANs are more abundant, possibly reflecting their lower rates of loss, a result of differing night-time versus daytime boundary layer meteorology–dynamics and chemical properties of the ANs formed.

Data availability. The PARADE data can be obtained on request (via John Crowley) from the owners. The NOTOMO data will be released at the end of 2017.

Competing interests. The authors declare that they have no conflict of interest.

Acknowledgements. We thank Heinz Bingemer for logistical support and use of the facilities at the Taunus Observatory during the NOTOMO and PARADE campaigns. We thank Horst Fischer for making the PARADE NO dataset available and the HLNUG for provision of meteorological data. We thank DuPont for provision of a sample of the FEP TE 9568 suspension used to coat the cavity walls. This work was carried out in part in fulfilment of the PhD of Nicolas Sobanski at the Johannes Gutenberg University in Mainz, Germany.

The article processing charges for this open-access publication were covered by the Max Planck Society.

Edited by: S. E. Pusede
Reviewed by: two anonymous referees

References

Atkinson, R.: Atmospheric chemistry of VOCs and NO_x, Atmos. Environ., 34, 2063–2101, 2000.

Atkinson, R. and Arey, J.: Gas-phase tropospheric chemistry of biogenic volatile organic compounds: a review, Atmos. Environ., 37, S197–S219, 2003a.

Atkinson, R. and Arey, J.: Atmospheric degradation of volatile organic compounds, Chem. Rev., 103, 4605–4638, doi:10.1021/cr0206420, 2003b.

Atlas, E.: Evidence for $>C_3$ alkyl nitrates in rural and remote atmosphere, Nature, 331, 426–428, 1988.

Ayres, B. R., Allen, H. M., Draper, D. C., Brown, S. S., Wild, R. J., Jimenez, J. L., Day, D. A., Campuzano-Jost, P., Hu, W., de Gouw, J., Koss, A., Cohen, R. C., Duffey, K. C., Romer, P., Baumann, K., Edgerton, E., Takahama, S., Thornton, J. A., Lee, B. H., Lopez-Hilfiker, F. D., Mohr, C., Wennberg, P. O., Nguyen, T. B., Teng, A., Goldstein, A. H., Olson, K., and Fry, J. L.: Organic nitrate aerosol formation via NO_3 + biogenic volatile organic compounds in the southeastern United States, Atmos. Chem. Phys., 15, 13377–13392, doi:10.5194/acp-15-13377-2015, 2015.

Beaver, M. R., Clair, J. M. St., Paulot, F., Spencer, K. M., Crounse, J. D., LaFranchi, B. W., Min, K. E., Pusede, S. E., Wooldridge, P. J., Schade, G. W., Park, C., Cohen, R. C., and Wennberg, P. O.: Importance of biogenic precursors to the budget of organic nitrates: observations of multifunctional organic nitrates by CIMS and TD-LIF during BEARPEX 2009, Atmos. Chem. Phys., 12, 5773–5785, doi:10.5194/acp-12-5773-2012, 2012.

Blanchard, P., Shepson, P. B., Schiff, H. I., and Drummond, J. W.: Development of a gas chromatograph for trace gas-chromatograph for trace-level measurement of peroxyacetyl nitrate using chemical amplification, Anal. Chem., 65, 2472–2477, doi:10.1021/ac00066a012, 1993.

Bonn, B., Bourtsoukidis, E., Sun, T. S., Bingemer, H., Rondo, L., Javed, U., Li, J., Axinte, R., Li, X., Brauers, T., Sonderfeld, H., Koppmann, R., Sogachev, A., Jacobi, S., and Spracklen, D. V.: The link between atmospheric radicals and newly formed parti-

cles at a spruce forest site in Germany, Atmos. Chem. Phys., 14, 10823–10843, doi:10.5194/acp-14-10823-2014, 2014.

Boyd, C. M., Sanchez, J., Xu, L., Eugene, A. J., Nah, T., Tuet, W. Y., Guzman, M. I., and Ng, N. L.: Secondary organic aerosol formation from the β-pinene+NO_3 system: effect of humidity and peroxy radical fate, Atmos. Chem. Phys., 15, 7497–7522, doi:10.5194/acp-15-7497-2015, 2015.

Browne, E. C., Perring, A. E., Wooldridge, P. J., Apel, E., Hall, S. R., Huey, L. G., Mao, J., Spencer, K. M., Clair, J. M. St., Weinheimer, A. J., Wisthaler, A., and Cohen, R. C.: Global and regional effects of the photochemistry of $CH_3O_2NO_2$: evidence from ARCTAS, Atmos. Chem. Phys., 11, 4209–4219, doi:10.5194/acp-11-4209-2011, 2011.

Browne, E. C., Min, K.-E., Wooldridge, P. J., Apel, E., Blake, D. R., Brune, W. H., Cantrell, C. A., Cubison, M. J., Diskin, G. S., Jimenez, J. L., Weinheimer, A. J., Wennberg, P. O., Wisthaler, A., and Cohen, R. C.: Observations of total $RONO_2$ over the boreal forest: NO_x sinks and HNO_3 sources, Atmos. Chem. Phys., 13, 4543–4562, doi:10.5194/acp-13-4543-2013, 2013.

Buhr, M. P., Parrish, D. D., Norton, R. B., Fehsenfeld, F. C., Sievers, R. E., and Roberts, J. M.: Contribution of Organic Nitrates to the Total Reactive Nitrogen Budget at a Rural Eastern U.S. Site, J. Geophys. Res., 95, 9809–9816, 1990.

Crowley, J. N., Schuster, G., Pouvesle, N., Parchatka, U., Fischer, H., Bonn, B., Bingemer, H., and Lelieveld, J.: Nocturnal nitrogen oxides at a rural mountain-site in south-western Germany, Atmos. Chem. Phys., 10, 2795–2812, doi:10.5194/acp-10-2795-2010, 2010.

Day, D. A., Wooldridge, P. J., Dillon, M. B., Thornton, J. A., and Cohen, R. C.: A thermal dissociation laser-induced fluorescence instrument for in situ detection of NO_2, peroxy nitrates, alkyl nitrates, and HNO_3, J. Geophys. Res.-Atmos., 107, 4046, doi:10.1029/2001jd000779, 2002.

Day, D. A., Dillon, M. B., Wooldridge, P. J., Thornton, J. A., Rosen, R. S., Wood, E. C., and Cohen, R. C.: On alkyl nitrates, O_3, and the "missing NOy", J. Geophys. Res.-Atmos., 108, 4501, doi:10.1029/2003jd003685, 2003.

Day, D. A., Wooldridge, P. J., and Cohen, R. C.: Observations of the effects of temperature on atmospheric HNO_3, ΣANs, ΣPNs, and NO_x: evidence for a temperature-dependent HO_x source, Atmos. Chem. Phys., 8, 1867–1879, doi:10.5194/acp-8-1867-2008, 2008.

Fahey, D. W., Hübler, G., Parrish, D. D., Williams, E. J., Norton, R. B., Ridley, B. A., Singh, H. B., Liu, S. C., and Fehsenfeld, F. C.: Reactive Nitrogen Species in the Troposphere: Measurements of NO, NO_2, HNO_3, Particulate Nitrate, Peroxyacetyl Nitrate (PAN), O_3, and Total Reactive Odd Nitrogen (NO_y) at Niwot Ridge, Colorado, J. Geophys. Res., 91, 9781–9793, 1986.

Flocke, F., Volz-Thomas, A., and Kley, D.: Measurements of alkyl nitrates in rural and polluted air masses, Atmos. Environ., 25, 1951–1960, 1991.

Flocke, F., Volz-Thomas, A., Buers, H. J., Patz, W., Garthe, H. J., and Kley, D.: Long-term measurements of alkyl nitrates in southern Germany 1. General behavior and seasonal and diurnal variation, J. Geophys. Res.-Atmos., 103, 5729–5746, 1998.

Fry, J. L., Kiendler-Scharr, A., Rollins, A. W., Brauers, T., Brown, S. S., Dorn, H. P., Dube, W. P., Fuchs, H., Mensah, A., Rohrer, F., Tillmann, R., Wahner, A., Wooldridge, P. J., and Cohen, R. C.: SOA from limonene: role of NO_3 in its generation and degradation, Atmos. Chem. Phys., 11, 3879–3894, doi:10.5194/acp-11-3879-2011, 2011.

Fry, J. L., Draper, D. C., Zarzana, K. J., Campuzano-Jost, P., Day, D. A., Jimenez, J. L., Brown, S. S., Cohen, R. C., Kaser, L., Hansel, A., Cappellin, L., Karl, T., Hodzic Roux, A., Turnipseed, A., Cantrell, C., Lefer, B. L., and Grossberg, N.: Observations of gas- and aerosol-phase organic nitrates at BEACHON-RoMBAS 2011, Atmos. Chem. Phys., 13, 8585–8605, doi:10.5194/acp-13-8585-2013, 2013.

Fry, J. L., Draper, D. C., Barsanti, K. C., Smith, J. N., Ortega, J., Winkle, P. M., Lawler, M. J., Brown, S. S., Edwards, P. M., Cohen, R. C., and Lee, L.: Secondary Organic Aerosol Formation and Organic Nitrate Yield from NO_3 Oxidation of Biogenic Hydrocarbons, Environ. Sci. Technol., 48, 11944–11953, doi:10.1021/es502204x, 2014.

Hallquist, M., Wangberg, I., Ljungstrom, E., Barnes, I., and Becker, K. H.: Aerosol and product yields from NO_3 radical-initiated oxidation of selected monoterpenes, Environ. Sci. Technol., 33, 553–559, doi:10.1021/es980292s, 1999.

Hallquist, M., Wenger, J. C., Baltensperger, U., Rudich, Y., Simpson, D., Claeys, M., Dommen, J., Donahue, N. M., George, C., Goldstein, A. H., Hamilton, J. F., Herrmann, H., Hoffmann, T., Iinuma, Y., Jang, M., Jenkin, M. E., Jimenez, J. L., Kiendler-Scharr, A., Maenhaut, W., McFiggans, G., Mentel, Th. F., Monod, A., Prévôt, A. S. H., Seinfeld, J. H., Surratt, J. D., Szmigielski, R., and Wildt, J.: The formation, properties and impact of secondary organic aerosol: current and emerging issues, Atmos. Chem. Phys., 9, 5155–5236, doi:10.5194/acp-9-5155-2009, 2009.

IUPAC: Task Group on Atmospheric Chemical Kinetic Data Evaluation, available at: http://iupac.pole-ether.fr/index.html (last access: January 2017), 2016.

Jacobs, M. I., Burke, W. J., and Elrod, M. J.: Kinetics of the reactions of isoprene-derived hydroxynitrates: gas phase epoxide formation and solution phase hydrolysis, Atmos. Chem. Phys., 14, 8933–8946, doi:10.5194/acp-14-8933-2014, 2014.

Kiendler-Scharr, A., Mensah, A. A., Friese, E., Topping, D., Nemitz, E., Prevot, A. S. H., Aijala, M., Allan, J., Canonaco, F., Canagaratna, M., Carbone, S., Crippa, M., Dall Osto, M., Day, D. A., De Carlo, P., Di Marco, C. F., Elbern, H., Eriksson, A., Freney, E., Hao, L., Herrmann, H., Hildebrandt, L., Hillamo, R., Jimenez, J. L., Laaksonen, A., McFiggans, G., Mohr, C., O'Dowd, C., Otjes, R., Ovadnevaite, J., Pandis, S. N., Poulain, L., Schlag, P., Sellegri, K., Swietlicki, E., Tiitta, P., Vermeulen, A., Wahner, A., Worsnop, D., and Wu, H. C.: Ubiquity of organic nitrates from nighttime chemistry in the European submicron aerosol, Geophys. Res. Lett., 43, 7735–7744, doi:10.1002/2016gl069239, 2016.

Kourtidis, K. A., Fabian, P., Zerefos, C., and Rappengluck, B.: Peroxyacetyl Nitrate (Pan), Peroxypropionyl Nitrate (Ppn) and Pan Ozone Ratio Measurements at 3 Sites in Germany, Tellus Ser. B, 45, 442–457, doi:10.1034/j.1600-0889.1993.t01-3-00004.x, 1993.

LaFranchi, B. W., Wolfe, G. M., Thornton, J. A., Harrold, S. A., Browne, E. C., Min, K. E., Wooldridge, P. J., Gilman, J. B., Kuster, W. C., Goldan, P. D., de Gouw, J. A., McKay, M., Goldstein, A. H., Ren, X., Mao, J., and Cohen, R. C.: Closing the peroxy acetyl nitrate budget: observations of acyl peroxy nitrates

(PAN, PPN, and MPAN) during BEARPEX 2007, Atmos. Chem. Phys., 9, 7623–7641, doi:10.5194/acp-9-7623-2009, 2009.

Lee, A. K. Y., Abbatt, J. P. D., Leaitch, W. R., Li, S.-M., Sjostedt, S. J., Wentzell, J. J. B., Liggio, J., and Macdonald, A. M.: Substantial secondary organic aerosol formation in a coniferous forest: observations of both day- and nighttime chemistry, Atmos. Chem. Phys., 16, 6721–6733, doi:10.5194/acp-16-6721-2016, 2016.

Lee, B. H., Mohr, C., Lopez-Hilfiker, F. D., Lutz, A., Hallquist, M., Lee, L., Romer, P., Cohen, R. C., Iyer, S., Kurten, T., Hu, W. W., Day, D. A., Campuzano-Jost, P., Jimenez, J. L., Xu, L., Ng, N. L., Guo, H. Y., Weber, R. J., Wild, R. J., Brown, S. S., Koss, A., de Gouw, J., Olson, K., Goldstein, A. H., Seco, R., Kim, S., McAvey, K., Shepson, P. B., Starn, T., Baumann, K., Edgerton, E. S., Liu, J. M., Shilling, J. E., Miller, D. O., Brune, W., Schobesberger, S., D'Ambro, E. L., and Thornton, J. A.: Highly functionalized organic nitrates in the southeast United States: Contribution to secondary organic aerosol and reactive nitrogen budgets, P. Natl. Acad. Sci. USA, 113, 1516–1521, doi:10.1073/pnas.1508108113, 2016.

Lee, L., Teng, A. P., Wennberg, P. O., Crounse, J. D., and Cohen, R. C.: On Rates and Mechanisms of OH and O-3 Reactions with Isoprene-Derived Hydroxy Nitrates, J. Phys. Chem. A, 118, 1622–1637, doi:10.1021/jp4107603, 2014.

Lelieveld, J., Gromov, S., Pozzer, A., and Taraborrelli, D.: Global tropospheric hydroxyl distribution, budget and reactivity, Atmos. Chem. Phys., 16, 12477–12493, doi:10.5194/acp-16-12477-2016, 2016.

Li, J., Reiffs, A., Parchatka, U., and Fischer, H.: In situ measurements of atmospheric CO and its correlation with NO_x and O_3 at a rural mountain site, Metrol. Meas. Sys., XXII, 25–38, 2015.

Murphy, J. G., Thornton, J. A., Wooldridge, P. J., Day, D. A., Rosen, R. S., Cantrell, C., Shetter, R. E., Lefer, B., and Cohen, R. C.: Measurements of the sum of HO_2NO_2 and $CH_3O_2NO_2$ in the remote troposphere, Atmos. Chem. Phys., 4, 377–384, doi:10.5194/acp-4-377-2004, 2004.

Murphy, J. G., Day, D. A., Cleary, P. A., Wooldridge, P. J., and Cohen, R. C.: Observations of the diurnal and seasonal trends in nitrogen oxides in the western Sierra Nevada, Atmos. Chem. Phys., 6, 5321–5338, doi:10.5194/acp-6-5321-2006, 2006.

Mutzel, A., Rodigast, M., Iinuma, Y., Boge, O., and Herrmann, H.: Monoterpene SOA – Contribution of first-generation oxidation products to formation and chemical composition, Atmos. Environ., 130, 136–144, doi:10.1016/j.atmosenv.2015.10.080, 2016.

Nah, T., Sanchez, J., Boyd, C. M., and Ng, N. L.: Photochemical Aging of alpha-pinene and beta-pinene Secondary Organic Aerosol formed from Nitrate Radical Oxidation, Environ. Sci. Technol., 50, 222–231, doi:10.1021/acs.est.5b04594, 2016.

Nault, B. A., Garland, C., Pusede, S. E., Wooldridge, P. J., Ullmann, K., Hall, S. R., and Cohen, R. C.: Measurements of $CH_3O_2NO_2$ in the upper troposphere, Atmos. Meas. Tech., 8, 987–997, doi:10.5194/amt-8-987-2015, 2015.

Ng, N. L., Brown, S. S., Archibald, A. T., Atlas, E., Cohen, R. C., Crowley, J. N., Day, D. A., Donahue, N. M., Fry, J. L., Fuchs, H., Griffin, R. J., Guzman, M. I., Herrmann, H., Hodzic, A., Iinuma, Y., Jimenez, J. L., Kiendler-Scharr, A., Lee, B. H., Luecken, D. J., Mao, J., McLaren, R., Mutzel, A., Osthoff, H. D., Ouyang, B., Picquet-Varrault, B., Platt, U., Pye, H. O. T., Rudich, Y., Schwantes, R. H., Shiraiwa, M., Stutz, J., Thornton, J. A., Tilgner, A., Williams, B. J., and Zaveri, R. A.: Nitrate radicals and biogenic volatile organic compounds: oxidation, mechanisms, and organic aerosol, Atmos. Chem. Phys., 17, 2103–2162, doi:10.5194/acp-17-2103-2017, 2017.

Nölscher, A. C., Williams, J., Sinha, V., Custer, T., Song, W., Johnson, A. M., Axinte, R., Bozem, H., Fischer, H., Pouvesle, N., Phillips, G., Crowley, J. N., Rantala, P., Rinne, J., Kulmala, M., Gonzales, D., Valverde-Canossa, J., Vogel, A., Hoffmann, T., Ouwersloot, H. G., Vilà-Guerau de Arellano, J., and Lelieveld, J.: Summertime total OH reactivity measurements from boreal forest during HUMPPA-COPEC 2010, Atmos. Chem. Phys., 12, 8257–8270, doi:10.5194/acp-12-8257-2012, 2012.

Nölscher, A. C., Bourtsoukidis, E., Bonn, B., Kesselmeier, J., Lelieveld, J., and Williams, J.: Seasonal measurements of total OH reactivity emission rates from Norway spruce in 2011, Biogeosciences, 10, 4241–4257, doi:10.5194/bg-10-4241-2013, 2013.

Olszyna, K. J., Bailey, E. M., Simonaitis, R., and Meagher, J. F.: O_3 and NO_y relationships at a rural Site, J. Geophys. Res.-Atmos., 99, 14557–14563, doi:10.1029/94jd00739, 1994.

Paulot, F., Crounse, J. D., Kjaergaard, H. G., Kroll, J. H., Seinfeld, J. H., and Wennberg, P. O.: Isoprene photooxidation: new insights into the production of acids and organic nitrates, Atmos. Chem. Phys., 9, 1479–1501, doi:10.5194/acp-9-1479-2009, 2009.

Perraud, V., Bruns, E. A., Ezell, M. J., Johnson, S. N., Greaves, J., and Finlayson-Pitts, B. J.: Identification of Organic Nitrates in the NO_3 Radical Initiated Oxidation of alpha-Pinene by Atmospheric Pressure Chemical Ionization Mass Spectrometry, Environ. Sci. Technol., 44, 5887–5893, doi:10.1021/es1005658, 2010.

Perring, A. E., Pusede, S. E., and Cohen, R. C.: An observational perspective on the atmospheric impacts of alkyl and multifunctional nitrates on ozone and secondary organic aerosol, Chem. Rev., 113, 5848–5870, doi:10.1021/cr300520x, 2013.

Phillips, G. J., Tang, M. J., Thieser, J., Brickwedde, B., Schuster, G., Bohn, B., Lelieveld, J., and Crowley, J. N.: Significant concentrations of nitryl chloride observed in rural continental Europe associated with the influence of sea salt chloride and anthropogenic emissions, Geophys. Res. Lett., 39, L10811, doi:10.1029/2012GL051912, 2012.

Ridley, B. A., Shetter, J. D., Walega, J. G., Madronich, S., Elsworth, C. M., Grahek, F. E., Fehsenfeld, F. C., Norton, R. B., Parrish, D. D., Hübler, G., Buhr, M., Williams, E. J., Allwine, E. J., and Westberg, H. H.: The Behavior of Some Organic Nitrates at Boulder and Niwot Ridge, Colorado, J. Geophys. Res., 95, 13949–13961, 1990.

Rindelaub, J. D., McAvey, K. M., and Shepson, P. B.: The photochemical production of organic nitrates from alpha-pinene and loss via acid-dependent particle phase hydrolysis, Atmos. Environ., 100, 193–201, doi:10.1016/j.atmosenv.2014.10.010, 2015.

Roberts, J. M.: The atmospheric chemistry of organic nitrates, Atmos. Environ., 24, 243–287, 1990.

Roberts, J. M., Fajer, R. W., and Springston, S. R.: Capillary gas-chromatographic separation of alkyl nitrates and peroxycarboxylic nitric anhydrides, Anal. Chem., 61, 771–772, doi:10.1021/ac00182a026, 1989.

Roberts, J. M., Bertman, S. B., Parrish, D. D., Fehsenfeld, F. C., Jobson, B. T., and Niki, H.: Measurement of alkyl nitrates at Chebogue Point, Nova Scotia during the 1993 North Atlantic Re-

gional Experiment (NARE) intensive, J. Geophys. Res.-Atmos., 103, 13569–13580, 1998.

Roberts, J. M., Marchewka, M., Bertman, S. B., Sommariva, R., Warneke, C., de Gouw, J., Kuster, W., Goldan, P., Williams, E., Lerner, B. M., Murphy, P., and Fehsenfeld, F. C.: Measurements of PANs during the New England air quality study 2002, J. Geophys. Res.-Atmos., 112, D20306, doi:10.1029/2007jd008667, 2007.

Rollins, A. W., Browne, E. C., Min, K.-E., Pusede, S. E., Wooldridge, P. J., Gentner, D. R., Goldstein, A. H., Liu, S., Day, D. A., Russell, L. M., and Cohen, R. C.: Evidence for NO_x Control over Nighttime SOA Formation, Science, 337, 1210–1212, 2012.

Rollins, A. W., Pusede, S., Wooldridge, P., Min, K. E., Gentner, D. R., Goldstein, A. H., Liu, S., Day, D. A., Russell, L. M., Rubitschun, C. L., Surratt, J. D., and Cohen, R. C.: Gas/particle partitioning of total alkyl nitrates observed with TD-LIF in Bakersfield, J. Geophys. Res.-Atmos., 118, 6651–6662, doi:10.1002/jgrd.50522, 2013.

Rosen, R. S., Wood, E. C., Wooldridge, P. J., Thornton, J. A., Day, D. A., Kuster, W., Williams, E. J., Jobson, B. T., and Cohen, R. C.: Observations of total alkyl nitrates during Texas Air Quality Study 2000: Implications for O_3 and alkyl nitrate photochemistry, J. Geophys. Res.-Atmos., 109, D07303, doi:10.1029/2003jd004227, 2004.

Russo, R. S., Zhou, Y., Haase, K. B., Wingenter, O. W., Frinak, E. K., Mao, H., Talbot, R. W., and Sive, B. C.: Temporal variability, sources, and sinks of C_1-C_5 alkyl nitrates in coastal New England, Atmos. Chem. Phys., 10, 1865–1883, doi:10.5194/acp-10-1865-2010, 2010.

Schrimpf, W., Linaerts, K., Muller, K. P., Koppmann, R., and Rudolph, J.: Peroxyacetyl nitrate (PAN) measurements during the POPCORN campaign, J. Atmos. Chem., 31, 139–159, doi:10.1023/A:1006004031055, 1998.

Schuster, G., Labazan, I., and Crowley, J. N.: A cavity ring down/cavity enhanced absorption device for measurement of ambient NO_3 and N_2O_5, Atmos. Meas. Tech., 2, 1–13, doi:10.5194/amt-2-1-2009, 2009.

Schwantes, R. H., Teng, A. P., Nguyen, T. B., Coggon, M. M., Crounse, J. D., St Clair, J. M., Zhang, X., Schilling, K. A., Seinfeld, J. H., and Wennberg, P. O.: Isoprene NO_3 Oxidation Products from the RO_2+HO_2 Pathway, J. Phys. Chem. A, 119, 10158–10171, doi:10.1021/acs.jpca.5b06355, 2015.

Sobanski, N., Schuladen, J., Schuster, G., Lelieveld, J., and Crowley, J. N.: A five-channel cavity ring-down spectrometer for the detection of NO_2, NO_3, N_2O_5, total peroxy nitrates and total alkyl nitrates, Atmos. Meas. Tech., 9, 5103–5118, doi:10.5194/amt-9-5103-2016, 2016a.

Sobanski, N., Tang, M. J., Thieser, J., Schuster, G., Pöhler, D., Fischer, H., Song, W., Sauvage, C., Williams, J., Fachinger, J., Berkes, F., Hoor, P., Platt, U., Lelieveld, J., and Crowley, J. N.: Chemical and meteorological influences on the lifetime of NO_3 at a semi-rural mountain site during PARADE, Atmos. Chem. Phys., 16, 4867–4883, doi:10.5194/acp-16-4867-2016, 2016b.

Thieser, J., Schuster, G., Schuladen, J., Phillips, G. J., Reiffs, A., Parchatka, U., Pöhler, D., Lelieveld, J., and Crowley, J. N.: A two-channel thermal dissociation cavity ring-down spectrometer for the detection of ambient NO_2, RO_2NO_2 and $RONO_2$, Atmos. Meas. Tech., 9, 553–576, doi:10.5194/amt-9-553-2016, 2016.

Williams, J., Roberts, J. M., Fehsenfeld, F. C., Bertman, S. B., Buhr, M. P., Goldan, P. D., Hubler, G., Kuster, W. C., Ryerson, T. B., Trainer, M., and Young, V.: Regional ozone from biogenic hydrocarbons deduced from airborne measurements of PAN, PPN, and MPAN, Geophys. Res. Lett., 24, 1099–1102, 1997.

Williams, J., Roberts, J. M., Bertman, S. B., Stroud, C. A., Fehsenfeld, F. C., Baumann, K., Buhr, M. P., Knapp, K., Murphy, P. C., Nowick, M., and Williams, E. J.: A method for the airborne measurement of PAN, PPN, and MPAN, J. Geophys. Res., 105, 28943–28960, 2000.

Wooldridge, P. J., Perring, A. E., Bertram, T. H., Flocke, F. M., Roberts, J. M., Singh, H. B., Huey, L. G., Thornton, J. A., Wolfe, G. M., Murphy, J. G., Fry, J. L., Rollins, A. W., LaFranchi, B. W., and Cohen, R. C.: Total Peroxy Nitrates (SPNs) in the atmosphere: the Thermal Dissociation-Laser Induced Fluorescence (TD-LIF) technique and comparisons to speciated PAN measurements, Atmos. Meas. Tech., 3, 593–607, doi:10.5194/amt-3-593-2010, 2010.

Worton, D. R., Reeves, C. E., Penkett, S. A., Sturges, W. T., Slemr, J., Oram, D. E., Bandy, B. J., Bloss, W. J., Carslaw, N., Davey, J., Emmerson, K. M., Gravestock, T. J., Hamilton, J. F., Heard, D. E., Hopkins, J. R., Hulse, A., Ingram, T., Jacob, M. J., Lee, J. D., Leigh, R. J., Lewis, A. C., Monks, P. S., and Smith, S. C.: Alkyl nitrate photochemistry during the tropospheric organic chemistry experiment, Atmos. Environ., 44, 773–785, 2010.

Xiong, F., McAvey, K. M., Pratt, K. A., Groff, C. J., Hostetler, M. A., Lipton, M. A., Starn, T. K., Seeley, J. V., Bertman, S. B., Teng, A. P., Crounse, J. D., Nguyen, T. B., Wennberg, P. O., Misztal, P. K., Goldstein, A. H., Guenther, A. B., Koss, A. R., Olson, K. F., de Gouw, J. A., Baumann, K., Edgerton, E. S., Feiner, P. A., Zhang, L., Miller, D. O., Brune, W. H., and Shepson, P. B.: Observation of isoprene hydroxynitrates in the southeastern United States and implications for the fate of NO_x, Atmos. Chem. Phys., 15, 11257–11272, doi:10.5194/acp-15-11257-2015, 2015.

Xu, L., Suresh, S., Guo, H., Weber, R. J., and Ng, N. L.: Aerosol characterization over the southeastern United States using high-resolution aerosol mass spectrometry: spatial and seasonal variation of aerosol composition and sources with a focus on organic nitrates, Atmos. Chem. Phys., 15, 7307–7336, doi:10.5194/acp-15-7307-2015, 2015.